Electronic supplementary information (ESI)

Enhanced piezotronics by single-crystalline ferroelectrics for uniformly strengthening the piezo-photocatalysis of electrospun $BaTiO_3$@TiO_2 nanofibers

Bi Fu [a, b, c] Jianjie Li [a], Huaide Jiang [a], Xiaoli He [a], Yanmei Ma [a], Jingke Wang [a], Chaoyang Shi*[d] and Chengzhi Hu *[a, c]

[a] Shenzhen Key Laboratory of Biomimetic Robotics and Intelligent Systems, Department of Mechanical and Energy Engineering, Southern University of Science and Technology, Shenzhen, 518055, China.

[b] School of Optoelectronic Engineering, Guangdong Polytechnic Normal University, Guangzhou 510665, China.

[C] Guangdong Provincial Key Laboratory of Human-Augmentation and Rehabilitation Robotics in Universities, Southern University of Science and Technology, Shenzhen, 518055, China.

[d] Key Laboratory of Mechanism Theory and Equipment Design of Ministry of Education, School of Mechanical Engineering, Tianjin University, Tianjin, 300072, China.

*Corresponding author. E-mail: hucz@sustech.edu.cn (C. Hu); chaoyang.shi@tju.edu.cn (C. Shi).

TGA analysis of $BaTiO_3/TiO_2$/PVP nanofibers. Fig. S1 shows the TGA curve of $BaTiO_3/TiO_2$/PVP precursor nanofibers that are annealed in the air with temperatures ranging from 50 to 800 °C. The weight of the precursor nanofibers steadily decreases with the increase of temperature. The minor mass loss between 50-300 °C is due to the removal of solvents. The second endothermic peak accompanied by the mass loss about 65% between 300-400 °C is attributed to the decomposition of PVP and butyl titanate. The mass loss in the temperature range of 400-500 °C is related to the decomposition of organic groups. About 92% mass loss is observed around 500 °C. There is no mass loss above 500 °C, which indicates the crystallization temperature. Thus, a temperature above 500 °C is used to anneal the $BaTiO_3/TiO_2$/PVP precursor nanofibers to ensure crystallization.

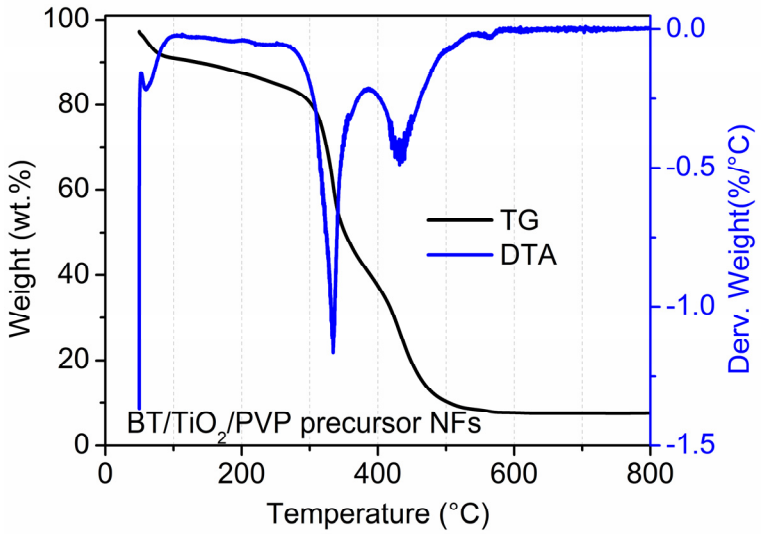

Figure S1. TGA curves of $BaTiO_3/TiO_2$/PVP precursor nanofibers at temperatures ranging from 50 to 800 °C.

TiO_2 nanofibers are fabricated by a sol-gel assisted electrospinning followed by annealing. First, 0.65 g tetrabutyl titanium is dissolved into 8 mL ethanol, then 3.0 g PVP is added to increase its viscosity. The obtained 0.2 M TiO_2 precursor solution is loaded into a 10 mL plastic syringe with a G-21 stainless-steel needle. The feeding rate is controlled at 0.3 mL h^{-1} by a syringe pump. The distance between the needle tip and the ground collector is fixed at 12 cm. The relative humidity is kept within 30% at room temperature. Under a high voltage of 14 kV, TiO_2/PVP precursor nanofibers are collected by an aluminum foil for 5 h. The as-spun precursor nanofibers are dried at 120 °C overnight. Finally, TiO_2 nanofibers are obtained by sintering the dried precursor nanofibers at 500 °C for 2 h at the heating and cooling rates of 2 °C min^{-1}.

Fig. S2 shows the SEM image of TiO_2 nanofibers with a diameter of approximately 250 nm. The TEM image in Fig. S2(b) reveals that the TiO_2 nanofiber is composed of nanocrystals with an average size of 5 nm. Fig. S2(c) shows the HR-TEM image obtained from the white box in Fig. S2(b). The interplanar crystal spacing of 2.4 Å is ascribed to the (004) crystallographic plane of TiO_2. The full (Fig. S2(d)) and electron (Fig. S2(e)) mapping images of single TiO_2 nanofiber is composed of the individual Ti (Fig. S2(f)) and O (Fig. S2(g)) element mappings. All element mappings exhibit a one-dimensional fibric outline that confirms the successful synthesis of TiO_2 nanofibers.

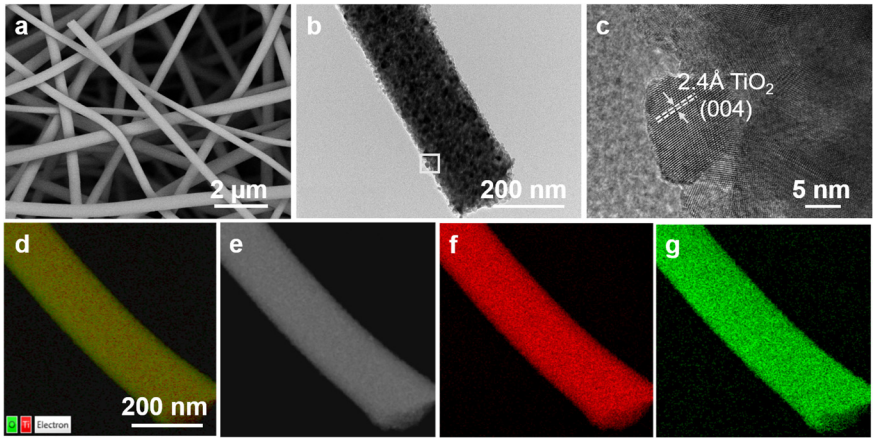

Figure S2. Morphology and microstructure of TiO_2 nanofibers. (a) SEM, (b) TEM, and (c) HR-TEM, (d) full, (e) electron, (f) Ti, and (g) O element mapping images of TiO_2 nanofibers.

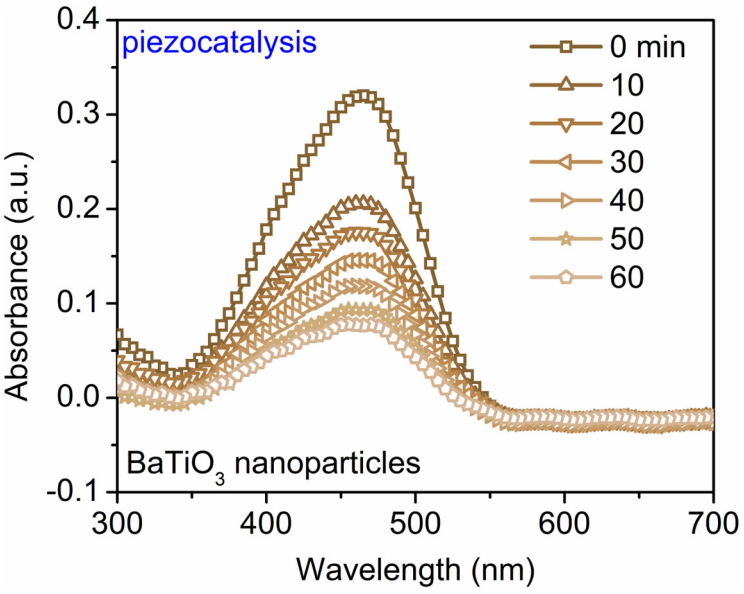

Figure S3. The UV-vis absorption spectra of $BaTiO_3$ nanoparticles under ultrasound irradiation.

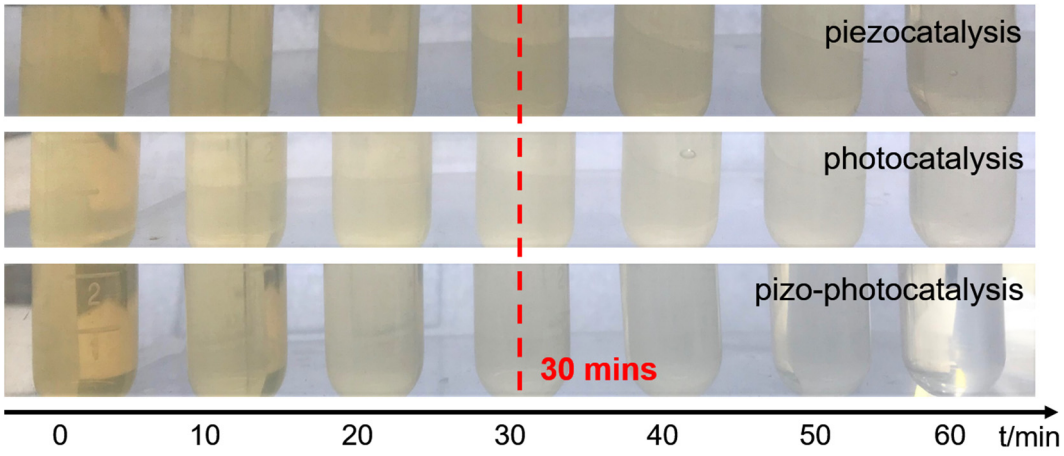

Figure S4. The photograph of the piezocatalytic, photocatalytic, and piezo-photocatalytic degradation of MO in water by $BaTiO_3$@TiO_2 hybrid nanofibers under ultrasound, UV light irradiation, and both ultrasound and UV light irradiation, respectively.

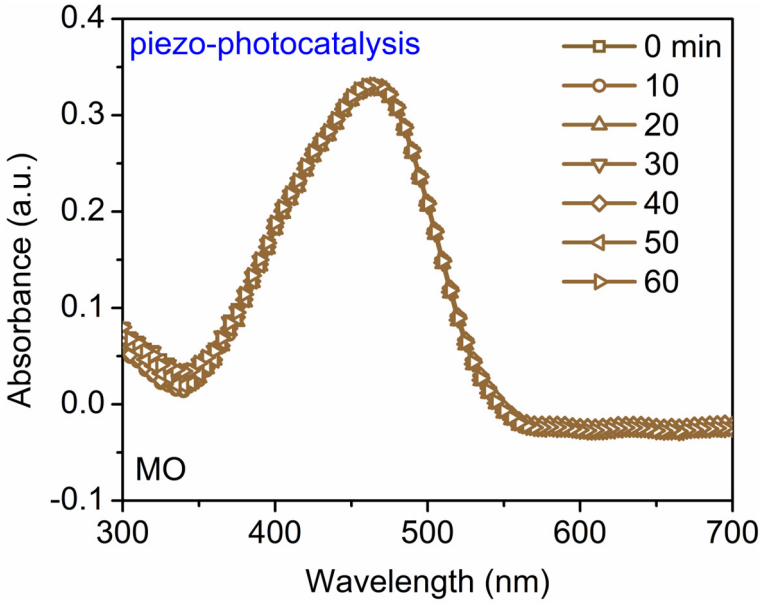

Figure S5. The UV-vis absorption spectra of the degradation of MO in water without catalysts under both ultrasound and UV light irradiation.

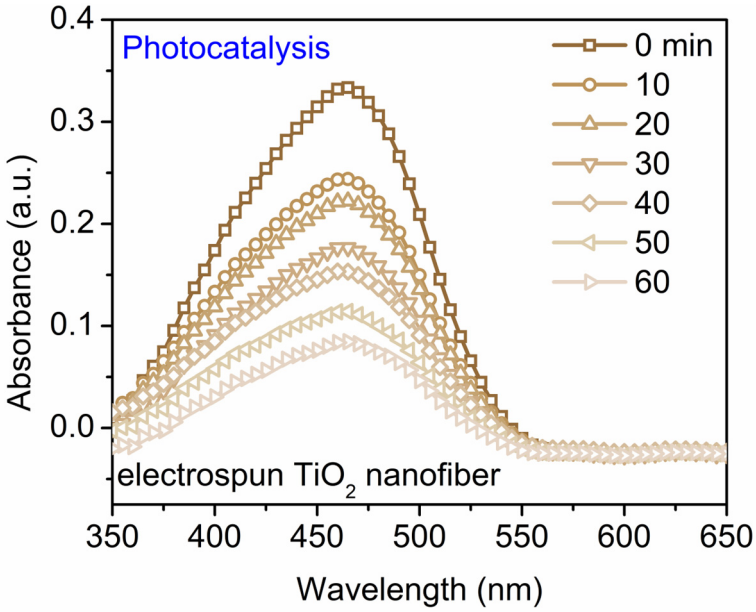

Figure S6. UV-vis absorption spectra of photocatalytic degradation of MO in water by TiO_2 nanofibers under the UV light irradiation.

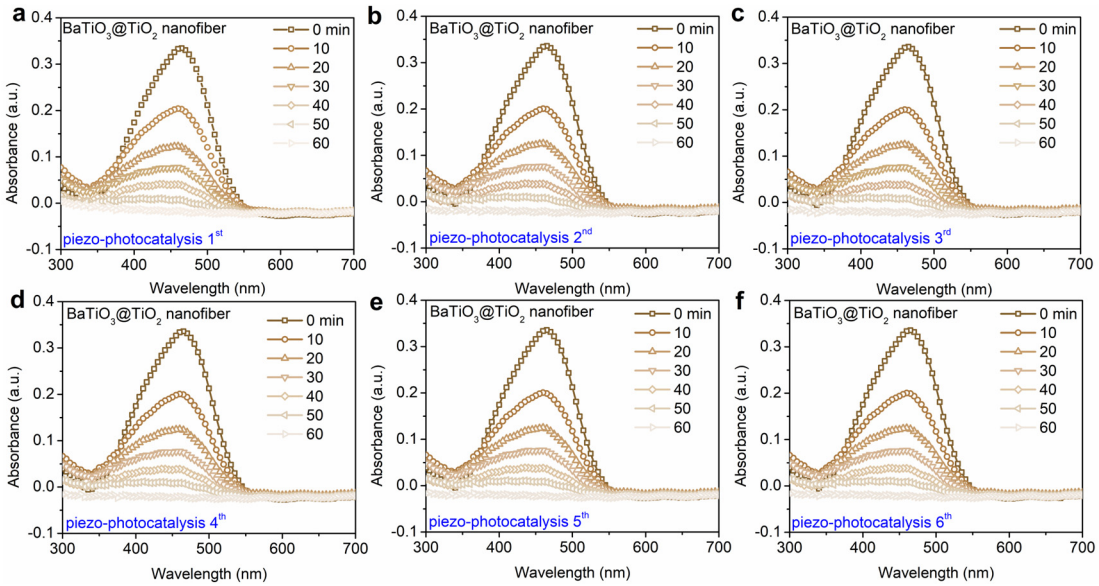

Figure S7. (a-f) UV-vis absorption spectra of the piezo-photocatalytic degradation of MO in water by $BaTiO_3$@TiO_2 hybrid nanofibers under both ultrasound and UV light irradiation in 6 cycles, respectively.